npj | 2D Materials and Applications

www.nature.com/npj2dmaterials

ARTICLE OPEN

Synthesis of ultrathin two-dimensional nanosheets and van der Waals heterostructures from non-layered γ-CuI

Kangkang Yao[1], Peng Chen[1,2], Zhengwei Zhang[1], Jia Li[1], Ruoqi Ai[1], Huifang Ma[1], Bei Zhao[1], Guangzhuang Sun[1], Ruixia Wu[1], Xuwan Tang[1], Bo Li[3], Jiawen Hu[1], Xidong Duan[1] and Xiangfeng Duan[2]

Two-dimensional (2D) nanosheets have attracted considerable recent interest for their atomically thin geometry and unique thickness-dependent electronic properties. The 2D nanosheets studied to date are generally limited to intrinsically layered materials, in which the covalently bonded atomic layers are held together by weak van der Waals forces and can be readily exfoliated to single or few-atom thick nanosheets. To prepare 2D nanosheets from non-layered materials can greatly expand the scope of 2D materials, but is much less straightforward. Here, we report the successful synthesis of ultrathin nanosheets from non-layered γ-CuI on SiO_2/Si substrate using a facile physical vapor deposition process. The resulting γ-CuI nanosheets display a triangular and hexagonal geometry with the lateral dimension up to 5 μm and thickness down to 1 nm. Raman spectroscopy, X-ray diffraction, and transmission electron microscopy studies demonstrate the resulting nanosheets retain single-crystalline γ-CuI phase. Additionally, we further show the γ-CuI nanosheets can be readily grown on other 2D materials (e.g., 2D-WSe_2, 2D-WS_2) to form van der Waals heterostructures (vdWHs). Optical microscopy images and Raman intensity mappings confirm the formation of γ-CuI/WS_2 and γ-CuI/WSe_2 vertical heterostructures. The electrical transport studies show that γ-CuI nanosheets exhibit a low resistivity of ~0.3 Ω cm and γ-CuI/WS_2 vertical heterostructures display a p-n diode behavior with distinct current rectification. The synthesis of γ-CuI nanosheets and heterostructures open a pathway to ultrathin nanosheets and van der Waals heterostructures from non-layered materials and could open up exciting opportunities in electronics and optoelectronics.

npj 2D Materials and Applications (2018)2:16 ; doi:10.1038/s41699-018-0058-2

INTRODUCTION

Two-dimensional (2D) materials have attracted significant attention as a new generation of atomically thin material for next-generation electronic and optoelectronic devices due to their ultrathin geometry and unique thickness-dependent physical properties. In the past decade, significant efforts have been devoted to synthesizing graphene[1] and graphene-like 2D materials including hexagonal BN,[2] transition metal dichalcogenides (TMDs) (such as MoS_2,[3] WS_2,[4] and WSe_2[5]), metal oxides (such as MoO_3,[6] WO_3[7]), and metal halides (such as PbI_2,[8] CdI_2,[9] BiI_3,[10] and CrI_3[11]) using various approaches. These 2D materials typically feature unconventional physical properties distinct from their bulk crystals, which can open up exciting opportunities for both the fundamental investigation of low dimensional chemistry and physics and potential technological applications at the limits of single atomic thickness.[12–21] Some available 2D materials may also be flexibly combined to produce new van der Waals heterostructures (vdWHs) with atomic sharp modulation of chemical composition and electronic structure. Such vdWHs can enable the creation of tailored heterojunctions without the traditional lattice matching requirement, and thus offer a much more flexible approach for heterogeneous material integration than the traditional semiconductor heterostructures. It can thus open up a limitless possibility to nearly arbitrarily combine and control different properties, and develop exciting new technologies beyond the reach of existing materials. Recent studies have already demonstrated the exciting potentials of 2D materials and vdWHs in nano-electronics applications, such as atomically thin transistors,[22,23] vertical field-effect transistors,[24] and optoelectronics applications, such as photodetectors[25] and light-emitting diodes.[26,27]

Although it has been relatively straightforward to produce ultrathin 2D nanosheets from intrinsically layered materials using various synthetic approaches, it is considerably more difficult to grow highly anisotropic ultrathin nanosheets from non-layered materials due to their intrinsic three-dimensional lattice structure. Nonetheless, a few examples of 2D nanosheets of some non-layered materials (such as ZnSe,[28] PbS[29]) and heterostructures (such as CdS/MoS_2,[30] PbS/MoS_2[31]) have been reported recently. Copper iodide (CuI), as a non-layered I–VII group compound, crystallizes into three different phases: α, β, and γ and shows different crystal lattices with increasing temperature. CuI undergoes a phase transition from the cubic γ-phase to the hexagonal β-phase above 369 °C. The β-phase can be further transformed to the cubic α-phase with increasing temperature above 407 °C.[32] Figure 1a, b is the stick-and-ball crystal structure model of γ-CuI. The low-temperature γ-phase CuI crystal is a p-type semiconductor[33] and has a cubic zinc blende structure with the space group F-43 m. In the crystal of γ-CuI, each Cu^+ ion is tetrahedrally surrounded by four I^- ions (Fig. 1a). Currently, γ-CuI has been

[1]State Key Laboratory for Chemo/Biosensing and Chemometrics, College of Chemistry and Chemical Engineering, Hunan University, 410082 Changsha, China; [2]Department of Chemistry and Biochemistry, University of California, Los Angeles 90095 CA, USA and [3]Department of Applied Physics, School of Physics and Electronics, Hunan University, 410082 Changsha, China
Correspondence: Jiawen Hu (jwhu@hnu.edu.cn) or Xidong Duan (xidongduan@hnu.edu.cn) or Xiangfeng Duan (xduan@chem.ucla.edu)

Received: 18 January 2018 Revised: 12 April 2018 Accepted: 16 April 2018

extensively applied in fields such as organic catalysts,[34] structural template of organic semiconductor,[35] solid state dye-sensitized solar cells[36,37] and hole conductor in perovskite solar cells.[38,39]

The preparations of γ-CuI nanoparticles,[40] nanowires,[41] thin films[42] have been studied using either physical or chemical methods. Furthermore, there are several reports on the synthesis of the γ-CuI single crystal nanoplates with the thickness of 60–90 nm via PEG/TSA-assisted solution-based methods.[43,44] However, the synthesis of regular and ultrathin γ-CuI nanosheets has not been reported. Here, we report a facile physical vapor deposition method to prepare high-quality single-crystalline γ-CuI nanosheets with the thickness down to 1 nm. Optical microscopy (OM), atomic force microscopy (AFM) and scanning electron microscopy (SEM) studies show triangular and hexagonal nanosheets can be readily grown on 300 nm SiO_2/Si substrate with the lateral dimension up to 5 μm and thicknesses down to 1 nm. Raman spectroscopy studies of the nanosheets reveal the transverse-optical (TO) mode of γ-CuI at around 122 cm^{-1}. X-ray diffraction (XRD) studies show highly crystalline nature of the obtained γ-CuI samples with cubic phase. Energy-dispersive X-ray spectroscopy (EDX) studies reveal that the atomic ratio between Cu and I is about 1:1. Transmission electron microscopy (TEM) and the corresponding selected area electron diffraction (SAED) studies demonstrate that the γ-CuI nanosheets are single crystalline. Take a step further, we also show that the γ-CuI nanosheets can also be readily grown on typical 2D materials to form γ-CuI/WSe_2 and γ-CuI/WS_2 van der Waals vertical heterostructures (vdWHs). The current–voltage curves show that γ-CuI nanosheets have low resistivity and γ-CuI/WS_2 vertical heterostructure show p–n diode behavior with distinct current rectification behavior.

RESULTS AND DISCUSSION

The γ-CuI nanosheets were synthesized on SiO_2/Si substrate using a home-built physical vapor deposition (PVD) system (Figure S1), with γ-CuI powder as the precursor and argon as the carrier gas. The as-synthesized γ-CuI nanosheets typically display a triangle shape and occasionally a hexagonal shape with lateral size in the range of 1–5 μm (Fig. 2a, Figure S2). The different γ-CuI nanosheets show highly distinct colors, which can be attributed to variable optical interference resulted from the different thicknesses. In addition to the relatively thick nanosheets with obvious contrast to the substrate color, there are a large number of triangular domains with rather weak contrast (highlighted by white arrows in Fig. 2a). The thickness of nanosheets ranges from 300 nm to 1 nm (Figure S2, Fig. 2b). Figure 2b further shows a high resolution OM image of an ultrathin γ-CuI nanosheet grown on the 300 nm SiO_2/Si substrate. The triangle nanosheet shows nearly the identical color with substrate due to its ultrathin thickness. The thickness can be further characterized using AFM. Figure 2c reveals the corresponding AFM image where the nanosheet has a

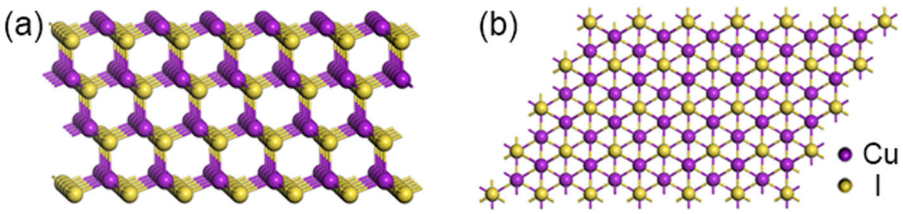

Fig. 1 Stick-and-ball crystal structures of γ-CuI. **a** Side view of the cubic crystal structure of γ-CuI along the (111) plane. **b** Top view of γ-CuI cubic crystal above the (111) plane. Purple and yellow spheres correspond to copper and iodine, respectively

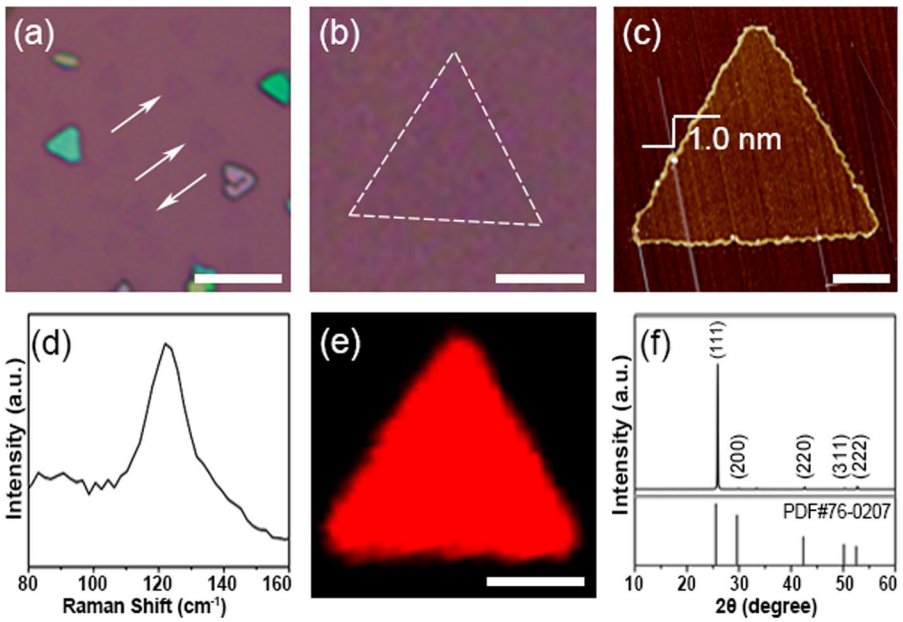

Fig. 2 The basic characterizations of γ-CuI nanosheets. **a** The OM image of the γ-CuI nanosheets grown on the SiO_2/Si substrate; The white arrows highlight the ultrathin nanosheets that are barely visible. Scale bar, 10 μm. **b**, **c** The OM image and AFM image of an ultrathin γ-CuI nanosheet. Scale bar, 2, 1 μm, respectively. **d** Raman spectrum of the γ-CuI nanosheets. Raman experiment was performed in a confocal spectrograph using a 532 nm excitation laser. **e** The Raman intensity mapping of a typical γ-CuI nanosheet with Raman peak located at 122 cm^{-1}. Scale bar, 2 μm. **f** XRD pattern of γ-CuI nanosheets grown on the SiO_2/Si substrate

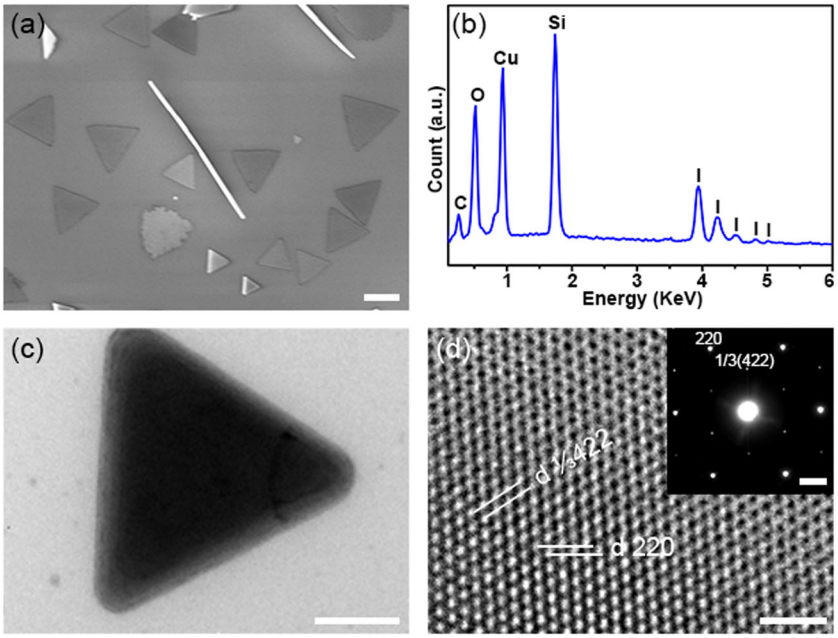

Fig. 3 SEM and TEM characterizations of γ-CuI nanosheets. **a** SEM image of triangular γ-CuI nanosheets grown on SiO_2/Si substrate; Scale bar, 1 μm. **b** SEM-EDX profile for the obtained γ-CuI nanosheets. **c** LR-TEM image of a typical triangle γ-CuI nanosheet supported on a grid of copper; Scale bar, 50 nm. **d** HR-TEM image of a γ-CuI nanosheet, the inset is the corresponding SAED pattern of the nanosheet; Scale bar, 2 nm, the scale bar in the inset is 2 1/nm

thickness of ~1 nm, indicating the formation of ultrathin 2D structure.

We have next conducted Raman and XRD studies on the resulted γ-CuI nanosheets (Fig. 2d–f). The Raman spectra of the resulted γ-CuI nanosheets exhibits a prominent characteristic peak around 122 cm^{-1} when excited with a 532 nm laser (Fig. 2d), in agreement with the TO mode of bulk γ-CuI at room temperature.[45] We were not able to observe the longitudinal-optical (LO) mode at 140 cm^{-1}, which can be interpreted by the reason that the LO peak may be sub-merged in the broad TO peak resulting from the existence of the disorder in the structure of γ-CuI.[46] A spatially resolved mapping of the Raman signal (122 cm^{-1}) shows highly uniform contrast throughout the entire nanosheet (Fig. 2e), suggesting highly uniform crystalline quality across the entire nanosheet. The XRD data indicates that the diffraction peaks can be indexed to cubic phase γ-CuI, which has a space group F-43 m with lattice parameters of $a = b = c = 6.034$ Å (JCPDS no. 76–0207) (Fig. 2f). A strong diffraction peak of the (111) plane suggests that the as-grown γ-CuI nanosheets tend to be preferentially oriented along the (111) direction. Additionally, the stability of γ-CuI nanosheets was also studied. Figure S3 shows the OM images and Raman spectra of freshly prepared CuI nanosheets and those obtained after a 5 days aging under ambient conditions. The nearly unchanged peak position and weakly reduced peak intensity indicate no significant degradation of the PVD-derived CuI nanosheets.

The synthesized γ-CuI nanosheets are further characterized using SEM and TEM studies (Fig. 3). A typical SEM image reveals the well-faceted triangular nanosheets deposited on SiO_2/Si substrate (Fig. 3a). The SEM-EDX spectroscopy demonstrates that the nanosheets consist of Cu and I elements (the exhibited O and Si elements are from the SiO_2 substrate), with the atomic ratio of Cu and I approximately 1 (Fig. 3b). Figure 3c shows the low-resolution TEM (LR-TEM) image of a typical γ-CuI nanosheet, where well-faced triangle shape of the nanosheet is clearly identified. The high-resolution TEM (HR-TEM) image of the nanosheet shows well-resolved lattice planes with a periodic atomic arrangement, confirming a single-crystalline nature of the resulted 2D nanosheets. The lattice spacing of 0.34 and 0.20 nm can be assigned to the 1/3(422) and (220) planes of cubic structure (Fig. 3d), respectively. The corresponding SAED pattern (inset of Fig. 3d) shows six-fold rotational symmetry for the diffraction spots, which can be indexed to the cubic-blend structure of γ-CuI along the [111] zone axis. The single set of diffraction spots further demonstrates the single crystalline nature of the γ-CuI nanosheets.

Furthermore, we also found that the γ-CuI nanosheets can be readily grown on 2D transition metal dichalcogenides (e.g., 2D-WSe_2, 2D-WS_2) to form vertical heterostructures by using a two-step PVD progress. Firstly, we grew the single-crystal WSe_2 (WS_2) nanosheets on the SiO_2/Si substrate using a PVD method.[24,47,48] Then, we directly grew the CuI nanosheets on the as-grown 2D-WSe_2 (WS_2) substrate (more details are described in the Methods). Interestingly, the γ-CuI nanosheets can readily nucleate and grow on the top surface of WSe_2 (WS_2) nanosheets, forming the γ-CuI/WSe_2 (γ-CuI/WS_2) vertical vdWHs (Fig. 4a–c). Figure 4a shows the OM image of the γ-CuI/WSe_2 vertical heterostructures, where the green and light gray domains are the γ-CuI nanosheets, and the purple domains are the underlying WSe_2 nanosheets. Figure 4b, c show optical images of the representative γ-CuI/WSe_2 and γ-CuI/WS_2 vertical heterostructures. It is noted that γ-CuI/WSe_2 and γ-CuI/WS_2 heterostructures apparently show a parallel orientation between the γ-CuI hexagonal domains and the underlying TMDs, suggesting a preferred van der Waals epitaxial relationship.[30] Figure 4d–f shows an optical image of a γ-CuI/WSe_2 vertical heterostructure, and the corresponding Raman mappings at 122 cm^{-1} (for γ-CuI) and 248 cm^{-1} (for WSe_2). The Raman studies clearly confirm the formation of vertical heterostructures. Besides, similar γ-CuI/WS_2 heterostructure have also clearly confirm the formation of vertical heterostructures (Fig. 4g–i). Photoluminescence (PL) spectra on the resulted γ-CuI/WSe_2 and γ-CuI/WS_2 heterostructures were shown in Fig. 4j, k. The results indicate that the WSe_2 and WS_2 monolayers exhibit strong PL emission with a dominant emission peak locating at 769 and 630 nm, respectively, whereas both γ-CuI/WSe_2 and γ-CuI/WS_2 regions show apparent PL quenching, with essentially no detectable PL. The observed quenching of the PL in the heterostructure may be attributed to

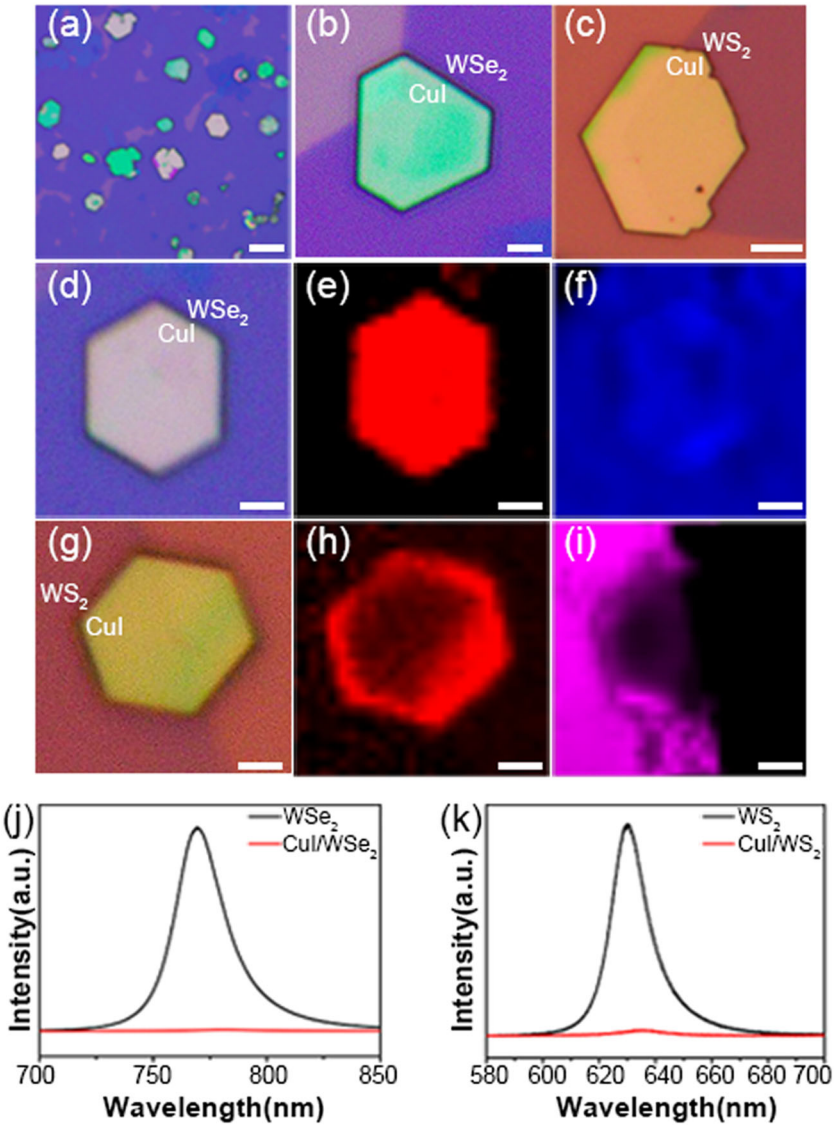

Fig. 4 OM, Raman, and PL characterizations of the γ-CuI/WSe_2 and γ-CuI/WS_2 heterostructures. **a** OM image of the γ-CuI/WSe_2 heterostructures on the SiO_2/Si substrate. Scale bar, 10 μm. **b**, **c** High magnification OM image of the representative γ-CuI/WSe_2 and γ-CuI/WS_2 vertical heterostructures. Scale bar, 5 and 2 μm, respectively. **d** OM image of a typical γ-CuI/WSe_2 vertical heterostructure used for Raman characterization. Scale bar, 2 μm. **e**, **f** Raman intensity mappings at 122 and 248 cm^{-1}, corresponding to the characteristic Raman peak of CuI and WSe_2, respectively. Scale bar, 2 μm. **g** OM image of a typical γ-CuI/WS_2 vertical heterostructure used for Raman characterization. Scale bar, 2 μm. **h**, **i** Raman intensity mappings at 122 and 350 cm^{-1}, corresponding to the characteristic Raman peak of CuI and WS_2, respectively. Scale bar, 2 μm. **j** PL spectra observed from bare WSe_2 region (black curve) and CuI/WSe_2 heterostructure region (red curve). **k** PL spectra observed from bare WS_2 region (black curve) and CuI/WS_2 heterostructure region (red curve).

the spontaneous separation of charge carriers in the junction region.[49,50]

We have further studied the electronic properties of the γ-CuI nanosheets and γ-CuI/WS_2 vertical heterostructure (Fig. 5). The insets of Fig. 5a, b show optical images of two γ-CuI nanosheets devices. The current–voltage (*I*–*V*) characteristic curves at room temperature show the linear and symmetric relationship, indicating that the good ohmic contacts are formed (Fig. 5a, b). The resulting γ-CuI nanosheets show a relatively low resistivity about 0.28 Ω cm for the 230 nm thick nanosheets and 0.57 Ω cm for the 43 nm nanosheets. The low resistivity of the γ-CuI nanosheets may be largely attributed to copper vacancy, acting as an electron acceptor that creates holes in the valence band.[51] Because γ-CuI is reported to be a p-type semiconductor, WSe_2 is an p-type semiconductor, and WS_2 is an n-type semiconductor,[47,51,52] the γ-CuI/WSe_2 vertical heterostructure may be formed a p–p junction whereas the γ-CuI/WS_2 vertical heterostructure is expected to behavior as a p–n diode. Figure S4 shows the band alignment and band diagram of CuI, WS_2, and WSe_2 across the heterostructure. At zero bias, the conduction band minimum and valence band maximum of CuI are located at a higher energy than that of WS_2, forming a type-II heterostructure. Thus, the electrons on the conduction band transfer from CuI to WS_2, while the holes on the valence band transfer from WS_2 to CuI resulting in the efficient charge separation. Indeed, the current–voltage characteristics of a typical γ-CuI/WS_2 vertical heterostructure show obvious current rectification behavior with a rectification ratio reaching up to 338 at the bias voltage of ±1.5 V (Fig. 5c), consistent with the expected p-n diode behavior. The inset shows the optical image of a typical device where the Au electrodes are separately made on γ-CuI and

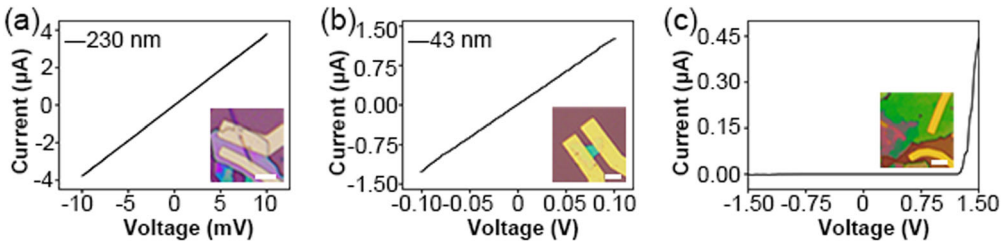

Fig. 5 Electrical characterization of the γ-CuI nanosheets and γ-CuI/WS_2 vertical heterostructure. **a** Current–voltage characteristic of the γ-CuI nanosheet with the thickness of 230 nm. **b** Current-voltage characteristic of the γ-CuI nanosheet with the thickness of 43 nm. **c** Current–voltage characteristic of the γ-CuI/WS_2 vertical heterostructure p-n diode. The inset shows the OM image of the corresponding devices. Scale bars, 5 μm

WS_2. We have further deduced the ideality factor using Lamber function:[53]

$$I(\mathrm{V}) = \frac{nV_\mathrm{T}}{R_\mathrm{S}} W_\mathrm{o}\left(\frac{I_\mathrm{S}R_\mathrm{S}}{nV_\mathrm{T}} \mathrm{e}^{(V+I_\mathrm{S}R_\mathrm{S})/nV_\mathrm{T}}\right) - I_\mathrm{S}, \quad (1)$$

where I_S is the saturation current, V_T is the thermal voltage (≈0.026 V at $T = 300$ K), n is the ideality factor, and R_S is the series resistance. An ideality factor $n = 2.72$ is extracted, which compares well with many other 2D diodes.[54,55]

In summary, we have reported the successful synthesis of ultrathin nanosheets from non-layered γ-CuI and 2D-γ-CuI/WSe_2, 2D-γ-CuI/WS_2 vdWHs on SiO_2/Si substrate using a facile PVD method. The obtained γ-CuI nanosheets exhibit triangle shapes and hexagonal shapes with lateral size up to several micrometers and thickness down to 1 nm. The Raman spectra studies show characteristic peak at around 122 cm^{-1}, in accordance with the bulk γ-CuI. XRD study suggests the obtained nanosheets are pure cubic phase of γ-CuI crystal with the (111) directions normal to the SiO_2/Si substrate plane. TEM and SAED studies demonstrate the high crystallinity and single crystal nature of the as-synthesized γ-CuI nanosheets. The γ-CuI/WSe_2 and γ-CuI/WS_2 vertical heterostructures have been prepared by a two-step PVD progress. The electrical transport studies show that γ-CuI nanosheets have low revisitivity ~0.3 Ω cm and γ-CuI/WS_2 vertical heterstructure show expected p–n diode behavior. The successful synthesis of 2D nanosheets from non-layered γ-CuI and van der Waals heterostructures opens a new path way to explore ultrathin 2D structure from other non-layered materials and could enable new opportunities for electronic and optoelectronic devices.

METHODS

Synthesis of single crystal γ-CuI nanosheets

The γ-CuI nanosheets were grown on 300 nm SiO_2/Si substrate using a home-built PVD system. Figure S1 shows the illustration of the PVD setup for γ-CuI growth. Briefly, 0.5 g CuI powder (Alfa, 99.5%) in a small ceramic boat was placed in the center of a horizontal tube furnace with 1-inch diameter quartz tube. The 300 nm SiO_2/Si substrate (~1 cm × 3 cm) was placed in another boat downstream about 10 cm away from the center of the quartz tube. Prior to the growth, the tube was purged with ~400 sccm Ar carrier gas (Rizhen, ~99.999%) flow for 10 min at room temperature to remove residual oxygen in the reactor. The furnace was then ramped to the desired growth temperature 360–410 °C, and kept for 10–40 min under ambient pressure with an argon gas flow of 100–225 sccm. Note that the temperature of the growth substrate at the downstream end is 193–234 °C when the center heating zone is set at 360–410 °C. The growth was terminated by shutting off the power of the furnace, and the system was naturally cooled down to room temperature.

Synthesis of WSe_2 and WS_2 nanosheets

WSe_2 nanosheets: A ceramic boat loaded with WSe_2 powder (Sigma Aldrich, 99.9%) was placed in the center of the furnace. A 300 nm SiO_2/Si substrate was placed face-up on the other boat downstream. Before heating, high-purity argon gas was continuously introduced into the quartz tube. The furnace was then heated to 1200 °C and a constant flow of 100 sccm Ar was used as carrier gas. Note that the temperature of the growth substrate at the downstream end is 782 °C when the center heating zone is set at 1200 °C. After stabilizing for 8 min, the growth was terminated by shutting off the power of the furnace, and the system was naturally cooled down to room temperature. WS_2 nanosheets: Similar to the growth of WS_2 nanosheets, a ceramic boat loaded with WS_2 powder (Sigma Aldrich, 99.9%) was placed into a ceramic boat at the center of the furnace. A 300 nm SiO_2/Si substrate was placed at the end of the furnace. During the growth of WSe_2 nanosheets, the furnace temperature was heated to 1180 °C in an argon environment and maintained 8 min with a 50 sccm of Ar as carrier gas. Note that the temperature of the substrate at the down stream end is about 754 °C when the center heating zone is set at 1180 °C. In the end, the growth was terminated by shutting off the power of the furnace, and the system was naturally reduced to room temperature.

Synthesis of 2D γ-CuI/WSe_2 and γ-CuI/WS_2 van der Waals heterostructures

The 2D γ-CuI/WSe_2 (γ-CuI/WS_2) vertical heterostructure was grown in an atmospheric pressure PVD system using CuI powder as the source. A ceramic boat loaded with CuI powder was placed into the heating zone of a quartz tube and the SiO_2/Si substrate with as grown WSe_2 (WS_2) nanosheets was placed at the downstream end of the tube furnace. The system was purged with high-purity Ar gas (Rizhen, ~99.999%) before ramping to the desired growth temperature for the growth of γ-CuI nanoplates at 450 °C, and maintained for 5 min with a 150 sccm of Ar as carrier gas. Note that the temperature of the substrate at the downstream end is at 262 °C when the center heating zone is set at 450 °C. Finally, the growth was terminated by shutting off the power of the furnace, and the system was naturally cooled down to room temperature.

Sample characterizations

The γ-CuI nanosheets grown on the SiO_2/Si substrate were first characterized using an optical microscope (DP27, OLYMPUS). The thickness of γ-CuI nanosheets was determined using an atomic force microscope (Bioscope system, BRUCKER). The crystal structure of the sample was studied using a X-ray diffraction spectrometer (XRD-6100, SHIMADZU). The morphology and element composition of the obtained γ-CuI nanosheets were characterized using a SEM microscope (ΣIGMA HD, ZEISS) equipped with an EDX system. TEM characterization was performed using a TEM microscope (JEM-2100F, JEOL), operating at 200 kV. Raman spectra from the γ-CuI nanosheets and the γ-CuI/WSe_2 (WS_2) heterostructures were collected using a confocal microscopic spectrometer (invia-reflex, Renishaw) with 532 nm laser as the excitation source.

Device fabrication and characterization

The γ-CuI nanosheet devices and p–n junction devices were fabricated using e-beam lithography and thermal evaporation of 150 nm Au electrode. The electrical measurements were done at room temperature under dark condition.

Data availability

The data related to the findings of this work are available from the corresponding author on reasonable request.

ACKNOWLEDGEMENTS

We acknowledge the financial support from the National Natural Science Foundation of China (No. 61528403 and No. 21673070) and the Fundamental Research Funds of the Central Universities (No. 531107051078).

AUTHOR CONTRIBUTIONS

X.D.D., J.H., and X.D. designed the research. K.Y. performed the synthesis and characterization of the samples. P.C. fabricated and measured the device. Z.Z. prepared the WS_2 and WSe_2 sample. All authors contributed to experiment research and commented on the manuscript.

ADDITIONAL INFORMATION

Supplementary information accompanies the paper on the *npj 2D Materials and Applications* website (https://doi.org/10.1038/s41699-018-0058-2).

Competing interests: The authors declare no competing interest.

Publisher's note: Springer Nature remains neutral with regard to jurisdictional claims in published maps and institutional affiliations.

REFERENCES

1. Novoselov, K. S. et al. Electric field effect in atomically thin carbon films. *Science* **306**, 666–669 (2004).
2. Jin, C., Lin, F., Suenaga, K. & Iijima, S. Fabrication of a freestanding boron nitride single layer and its defect assignments. *Phys. Rev. Lett.* **102**, 195505 (2009).
3. Wang, X., Feng, H., Wu, Y. & Jiao, L. Controlled synthesis of highly crystalline MoS_2 flakes by chemical vapor deposition. *J. Am. Chem. Soc.* **135**, 5304–5307 (2013).
4. Song, J.-G. et al. Layer controlled wafer-scale and conformal synthesis of tungesten disulfide nanosheets using atomic layer deposition. *ACS Nano* **7**, 11333–11340 (2013).
5. Chen, Y.-Z. et al. Ultrafast and low temperature synthesis of highly crystalline and patternable few-layers tungsten diselenide by laser irradiation assisted selenization process. *ACS Nano* **9**, 4346–4353 (2015).
6. Alsaif, M. M. et al. Tunable plasmon resonances in two-dimensional molybdenum oxide nanoflakes. *Adv. Mater.* **26**, 3931–3937 (2014).
7. Yan, J. et al. Tungsten oxide single crystal nanosheets for enhanced multichannel solar light harvesting. *Adv. Mater.* **27**, 1580–1586 (2015).
8. Wang, Y., Sun, Y.-Y., Zhang, S., Lu, T.-M. & Shi, J. Band gap engineering of a soft inorganic compound PbI_2 by incommensurate van der Waals epitaxy. *Appl. Phys. Lett.* **108**, 013105 (2016).
9. Ai, R. Q. et al. Growth of single-crystalline cadmium iodide nanoplates, CdI_2/MoS_2 (WS_2, WSe_2) van der Waals heterostructures, and patterned arrays. *ACS Nano* **11**, 3413–3419 (2017).
10. Li, J. et al. Synthesis of 2D layered BiI_3 nanoplates, BiI_3/WSe_2 van der Waals heterostructures and their electronic, optoelectronic properties. *Small* **13**, 1701034 (2017).
11. Huang, B. et al. Layer-dependent ferromagnetism in a van der Waals crystal down to the monolayer limit. *Nature* **546**, 270–273 (2017).
12. Liu, X. et al. High performance field-effect transistor based on multilayer tungsten disulfide. *ACS Nano* **8**, 10396–10402 (2014).
13. Huang, Y. et al. Designing the shape evolution of $SnSe_2$ nanosheets and their optoelectronic properties. *Nanoscale* **7**, 17375–17380 (2015).
14. Zhou, J. et al. Controlled synthesis of high-quality monolayered α-In_2Se_3 via physical vapor deposition. *Nano Lett.* **15**, 6400–6405 (2015).
15. Chow, W. L. et al. High mobility 2D palladium diselenide field-effect transistors with tunable ambipolar characteristics. *Adv. Mater.* **29**, 1602969 (2017).
16. Zhou, C. et al. Carrier type control of WSe_2 field-effect transistors by thickness modulation and MoO_3 layer doping. *Adv. Funct. Mater.* **26**, 4223–4230 (2016).
17. Ren, X. et al. Environmentally robust black phosphorus nanosheets in solution: application for self-powered photodetector. *Adv. Funct. Mater.* **27**, 1606834 (2017).
18. Cheng, L. et al. Ultrathin WS_2 nanoflakes as a high-performance electrocatalyst for the hydrogen evolution reaction. *Angew. Chem. Int. Ed.* **53**, 7860–7863 (2014).
19. Chuang, H. J. et al. Low-resistance 2D/2D Ohmic contacts: a universal approach to high-performance WSe_2, MoS_2, and $MoSe_2$ transistors. *Nano Lett.* **16**, 1896–1902 (2016).
20. Movva, H. C. P. et al. High-mobility holes in dual-gated WSe_2 field-effect transistors. *ACS Nano* **9**, 10402–10410 (2015).
21. Zhao, H. et al. Interlayer interactions in anisotropic atomically thin rhenium diselenide. *Nano Res.* **8**, 3651–3661 (2015).
22. Yu, Z. et al. Analyzing the carrier mobility in transition-metal dichalcogenide MoS_2 field-effect transistors. *Adv. Funct. Mater.* **27**, 1604093 (2017).
23. Radisavljevic, B., Radenovic, A., Brivio, J., Giacometti, V. & Kis, A. Single-layer MoS_2 transistors. *Nat. Nanotechnol.* **6**, 147–150 (2011).
24. Georgiou, T. et al. Vertical field-effect transistor based on graphene-WS_2 heterostructures for flexible and transparent electronics. *Nat. Nanotechnol.* **8**, 100–103 (2013).
25. Hu, P. et al. Highly responsive ultrathin GaS nanosheet photodectors on grid and flexible substrates. *Nano Lett.* **13**, 1649–1654 (2013).
26. Cheng, R. et al. Electroluminescence and photocurrent generation from atomically sharp WSe_2/MoS_2 heterojunction p-n diodes. *Nano Lett.* **14**, 5590–5597 (2014).
27. Murali, K., Dandu, M, & Majumdar, K. Gate-tunable $WSe_2/SnSe_2$ backward diode with ultrahigh-reverse rectification ratio. *ACS Appl. Mater. Interfaces* **10**, 5657–5664 (2018).
28. Sun, Y. et al. Fabrication of flexible and freestanding zinc chalcogenide single layers. *Nat. Commun.* **3**, 1057 (2012).
29. Acharya, S. et al. A bottom-up approach toward fabrication of ultrathin PbS sheets. *Nano Lett.* **13**, 409–415 (2013).
30. Zheng, W. et al. Anisotropic growth of nonlayered CdS on MoS_2 monolayer for functional vertical heterostructures. *Adv. Funct. Mater.* **26**, 2648–2654 (2016).
31. Wen, Y. et al. Integrated high-performance infrared phototransistor arrays composed of nonlayered PbS-MoS_2 heterostructures with edge contacts. *Nano Lett.* **16**, 6437–6444 (2016).
32. Miyake, S., Hoshino, S. & Takenaka, T. On the phase transition in cuprous iodide. *J. Phys. Soc. Jpn* **7**, 19–24 (1952).
33. Wang, J., Li, J. & Li, S.-S. Native p-type transparent conductive CuI via intrinsic defects. *J. Appl. Phys.* **110**, 054907 (2011).
34. Xu, H. J. et al. CuI-nanoparticles-catalyzed selective synthesis of phenols, anilines, and ihiophenols from aryl halides in aqueous solution. *J. Org. Chem.* **76**, 2296–2300 (2011).
35. Rochford, L. A. et al. Structural templating in a nonplanar phthalocyanine using single crystal copper iodide. *Adv. Mater. Interfaces* **2**, 1400540 (2015).
36. Kumara, G. R. A., Konno, A., Shiratsuchi, K., Tsukahara, J. & Tennakone, K. Dye-sensitized solid-state solar cells: use of crystal growth inhibitors for deposition of the hole collector. *Chem. Mater.* **14**, 954–955 (2002).
37. Yum, J. H., Chen, P., Gratzel, M. & Nazeeruddin, M. K. Recent developments in solid-state dye-sensitized solar cells. *ChemSusChem* **1**, 699–707 (2008).
38. Sun, W. et al. Room-temperature and solution-processed copper iodide as the hole transport layer for inverted planar perovskite solar cells. *Nanoscale* **8**, 15954–15960 (2016).
39. Christians, J. A., Fung, R. C. & Kamat, P. V. An inorganic hole conductor for organo-lead halide perovskite solar cells. improved hole conductivity with copper iodide. *J. Am. Chem. Soc.* **136**, 758–764 (2014).
40. Sharma, B. & Rabinal, M. K. Ambient synthesis and optoelectronic properties of copper iodide semiconductor nanoparticles. *J. Alloy Compd.* **556**, 198–202 (2013).
41. Meng, L.-R. et al. Synthesis of luminescent cubic phase one-dimensional CuI nanostructures in solution. *Cryst. Growth Des.* **10**, 3387–3390 (2010).
42. Kang, H., Liu, R., Chen, K., Zheng, Y. & Xu, Z. Electrodeposition and optical properties of highly oriented γ-CuI thin films. *Electrochim. Acta* **55**, 8121–8125 (2010).
43. Xu, Y., Chen, D., Jiao, X. & Ba, L. PEG-assisted fabrication of single-crystalline CuI nanosheets: a general route to two-dimensional nanostructured materials. *J. Phys. Chem. C* **111**, 6–9 (2007).
44. Zhang, B. et al. Morphogenesis of CuI nanocrystals by a TSA-assisted photochemical route: synthesis, optical properties, and growth mechanism. *Eur. J. Inorg. Chem.* **2009**, 1376–1384 (2009).
45. Burns, G., Dacol, F. H., Shafer, M. W. & Alben, R. The Raman spectra of the superionic conductor CuI in its three phases. *Solid State Commun.* **24**, 753–757 (1977).
46. Kaushik, D. K., Selvaraj, M., Ramu, S. & Subrahmanyam, A. Thermal evaporated copper iodide (CuI) thin films: a note on the disorder evaluated through the temperature dependent electrical properties. *Sol. Energy Mater. Sol. Cells* **165**, 52–58 (2017).
47. Zhou, H. et al. Large area growth and electrical properties of p-type WSe_2 atomic layers. *Nano Lett.* **15**, 709–713 (2014).
48. Elías, A. L. et al. Controlled synthesis and transfer of large-area WS_2 sheets: from single layer to few layers. *ACS Nano* **7**, 5235–5242 (2013).
49. Li, X. et al. Two-dimensional GaSe/$MoSe_2$ misfit bilayer heterojunctions by van der Waals epitaxy. *Sci. Adv.* **2**, e1501882 (2016).
50. Lee, C. H. et al. Atomically thin p–n junctions with van der Waals heterointerfaces. *Nat. Nanotechnol.* **9**, 676–681 (2014).
51. Yamada, N., Ino, R. & Ninomiya, Y. Truly transparent p-type γ-CuI thin films with high hole mobility. *Chem. Mater.* **28**, 4971–4981 (2016).

52. Duan, X. et al. Lateral epitaxial growth of two-dimensional layered semiconductor heterojunctions. *Nat. Nanotechnol.* **9**, 1024–1030 (2014).
53. Banwell, T. C. & Jayakumar, A. Exact analytical solution for current flow through diode with series resistance. *Electron. Lett.* **36**, 291–292 (2000).
54. Deng, Y. et al. Black phosphorus-monolayer MoS_2 van der Waals Heterojunction p-n Diode. *ACS Nano* **8**, 8292–8299 (2014).
55. Yu, W. J. et al. Vertically stacked multi-heterostructures of layered materials for logic transistors and complementary inverters. *Nat. Mater.* **12**, 246–252 (2013).